Pressure-induced metallization and robust superconductivity in pristine 1T-HfSe$_2$

S. Rahman [a,b,e], H. Saqib [b], X. Liang [a], D. Errandonea [c], A.S. Resta [b], A. Molina-Sanchez [d], G. Gao [a,**], L. Wang [a,*], Y. Tian [a], H-K. Mao [b]

[a] Center for High Pressure Science (CHiPS), State Key Laboratory of Metastable Materials Science and Technology, Yanshan University, Qinhuangdao, Hebei, 066004, China
[b] Center for High Pressure Science and Technology Advanced Research, Shanghai, 201203, China
[c] Departamento de Física Aplicada-ICMUV, MALTA Consolider Team, Universidad de Valencia, Edificio de Investigación, C/Dr. Moliner 50, Burjassot, 46100, Valencia, Spain
[d] Institute of Materials Science (ICMUV), University of Valencia, Catedratico Beltran 2, E-46980, Valencia, Spain
[e] School of Physics and Optoelectronic Engineering, University of Chinese Academy of Sciences, China

ARTICLE INFO

ABSTRACT

The two-dimensional semiconductor 1T-HfSe$_2$ is found to have highly tunable transport properties under pressure including metallization and pressure-driven superconductivity. The temperature-dependent resistivity of the sample suggests that a charge-density wave (CDW) state exists at low pressures in HfSe$_2$, but it is suppressed below 20 GPa. It is further found that metallization takes place at ~24 GPa followed by the appearance of a superconducting state at 26 GPa with a T_c of 6.7 K. Upon further compression to 33 GPa, the T_c increases monotonically to 7.5 K. Raman spectra, x-ray diffraction, transport measurements, and density-functional theory calculations suggest that the occurrence of the pressure-induced metallization and superconducting transition are intimately linked to a structural phase transition from the trigonal (P $\overline{3}$ m1) to a hexagonal structure ($P6_3/mmc$). Because of the phase transition, a massive structural reconstruction, and substantial band-structure changes around the Fermi level take place, which are due to the modification of weak van der Waals forces. The pressure-induced manipulation of the transport properties of 1T-HfSe$_2$ could provide crucial information towards its practical applications.

1. Introduction

Due to their rich physical characteristics and promising potential applications [1,2], especially in electronics and optoelectronics, transition metal dichalcogenides (TMDs) [3] have attracted tremendous attention as a new class of two-dimensional (2D) materials in the fields of material sciences and condensed matter physics. Layered TMDs with chemical formula MX$_2$ (M = Ti, Nb, Ta, Mo, Hf, W; X = S, Se, Te) exist in two basic structural polymorphs called (2H) and (1T). They consist of layers of metals atoms in trigonal prismatic (2H) or octahedral (1T) coordination [4,5]. Most of these materials exhibit charge-density wave (CDW) [3], which usually competes with superconductivity when tuning the crystalline and electronic structure by various methods [6]. Superconductivity is expected to appear if the CDW state of a TMD could be suppressed by external stimuli such as high compression.

The electronic structure of TMDs has mainly been tuned either by applying an electrical field to manage the spin splitting [7–10], using quantum confinement by controlling the samples thickness [8,11,12], or employing pressure in combination with temperature [4,13,14]. Employing stress or strain is another way to tune the electronic structure of TMDs [12,15]. However, being key state parameters, temperature and pressure are the most efficient and clean tools for tuning the structural framework as well as electronic states because they have the advantage of not introducing chemical disorder [13,14]. In different TMDs materials various pressure-induced electronic modifications, including semiconductor-to-metal transitions, have been observed [13,16,17]. Among the TMDs, HfSe$_2$ is a narrow band-gap semiconductor and has been proposed to be a competitor of silicon in semiconductor technology

* Corresponding author.
** Corresponding author.

[18]. In particular, 1T-HfSe$_2$ has a high electron affinity and an optical band gap well-matched with the solar spectrum, which makes it a promising candidate material for a high-performance field-effect transistor component [19], photovoltaic cells, and infrared optoelectronic devices [20]. Very recently metallization was proposed in HfSe$_2$ at ~10 GPa, which is to date the lowest metallization pressure among TMDs [16,17]. However, the conclusion was based upon transmittance measurements [16] which do not confirm the closure of the band gap and are consistent with a narrow band-gap semiconductor rather than with a metallic state. Zhang et al. also reported metallization from resistance measurements at room temperature, but the reported values for the resistivity [17] are too large to support metallization. In fact, the resistance reported at 10 GPa is at level of tens of ohms [17], which corresponds to a semimetal or a narrow band-gap semiconductor but not to a metal. In addition, no temperature-dependent resistance has been reported at 10 GPa to confirm the metallic nature of HfSe$_2$. All these facts are in apparent contradiction with claims of metallization, indicating that further high-pressure (HP) studies with solid evidence are needed to fully understand the HP behavior of HfSe$_2$. Moreover, there are no previous studies on a possible pressure-driven superconductivity in HfSe$_2$ and its pressure-temperature phase diagram has not been explored yet. On another hand, several recent studies suggest that tuning the band structure or carrier densities will be essential for many of its potential applications, including optoelectronics devices [21]. These reasons motivate us to explore the band structure, as well as precise characterize structural, electrical, vibrational, and optical properties of HfSe$_2$ using compressive strain.

In this article, we have performed a systematic HP study of 1T-HfSe$_2$ by combining resistivity, Raman scattering, and synchrotron X-ray diffraction (XRD) measurements under compression with density-functional theory calculations. At low-pressure 1T-HfSe$_2$ is a semiconductor, presenting a CDW order, as previously observed in other TMDs. The CDW order is suppressed below 20 GPa, followed by pressure-induced metallization and the appearance of superconductivity by cooling below 7 K. Notice that metallization occurs at 24 GPa and not at 10 GPa as reported before [16,17]. Structural and spectroscopic results suggested that a first-order structural phase transition from a trigonal (P$\overline{3}$m1) to a hexagonal structure (*P*6$_3$/mmc) at around 24 GPa is responsible for the above-mentioned changes. The superconducting transition temperature (T_c) increases from 6.6 K at 26 GPa to 7.5 K at 38 GPa. Finally, a phase diagram of 1T-HfSe$_2$ as function of pressure and temperature is mapped out, which reveals pressure-induced superconductivity that is closely linked to the emergence of the structural phase transition.

2. Experimental and calculation details

2.1. Sample growth and high-pressure experiments

High-purity 1T-HfSe$_2$ crystals were purchased from HQ-graphene. Diamond-anvil cells (DAC) with 300 μm culets were used to generate pressure up to 35 GPa. A ruby ball and Au foil were used to calibrate pressure [22,23]. Raman measurements were performed using an inVia Renishaw Raman spectrometer system with a laser wavelength of 532 nm and a grating of 1200 l/mm. Silicon oil was used as a pressure-transmitting medium (PTM) in HP XRD and Raman measurements. High-pressure synchrotron XRD measurements were conducted on the BL10XU beam line of Spring-8 synchrotron. Electrical transport measurements were carried out using a DAC made of non-magnetic Cu–Be alloy. An insulated gasket was prepared with a mixture of epoxy and cubic boron nitride for electrical measurements. Room-temperature and low temperature electrical resistivity of the samples were measured using a Keithley Source-meter 2410 and a physical property measurement system (DynaCool, Quantum Design Inc.) respectively. More details of the experiments are provided in the Supplemental Material (Note 1). To conclude the description of experiments we would like to state that we are aware that the used pressure media become non-hydrostatic in the pressure range covered by experiments [24,25]. However, the agreement achieved by experiments made with different techniques (using different PTM) and with computer simulations (assuming hydrostatic conditions) suggests that non-hydrostaticity does not play an efficient role in HfSe$_2$ a role as relevant as in other materials.

2.2. Calculations

Density-functional theory (DFT) calculations were performed to complete the experiments. Structure searches were performed using the particle swarm optimization technique as implemented in the CALYPSO code [26,27]. Structural relaxations were based on DFT within the Perdew-Burke-Ernzerhof (PBE) parametrization of the generalized gradient approximation [28] as implemented in the Vienna ab initio simulation package [29]. Band-structure, phonon, and electron-phonon coupling (EPC) calculations were also carried out using the QUANTUM ESPRESSO code [30], where norm-conserving pseudopotentials for Hf and Se with a kinetic energy cutoff of 70 Ry were employed. The Brillouin zone (BZ) was sampled using a 40 × 40 × 26 Monkhorst-Pack grid. For the band-structure HSE hybrid functionals [31] were used because HSE gives a more accurate determination of the band-gap energy than PBE, in particular, for systems where van der Waals forces are not negligible. In all calculations we considered the following electrons as valence: 5d and 6s of Hf and 4s and 4p of Se. Geometry relaxations were performed by imposing a tolerance on the atomic forces of 0.005 eV Å^{-1}. The obtained energies were converged to within 0.5 meV per formula unit by using these technical parameters.

3. Results and discussion

3.1. CDW and pressure-induced superconductivity

Layered 1T-HfSe$_2$ is a semiconductor with an indirect band gap of 0.8–1.1 eV [18,32,33]. Fig. 1 shows the resistivity of the sample as a function of pressure at room temperature (a) and during cooling at different pressure (b). The resistivity of HfSe$_2$ enormously decreases upon compression from ambient pressure to about 16 GPa and 24 GPa in two steps and then asymptotically approaches the minimum value reached at 35 GPa. The value of the resistivity at ambient conditions indicates that the material is an intrinsic semiconductor and, therefore, resistivity is proportional to Ref. $e^{E_{gap}/2K_BT}$[34] where E$_{gap}$ is the band-gap energy and K$_B$ is the Boltzmann constant. Thus, a decrease of band-gap energy will explain the observed decrease of the resistivity up to 15 GPa. This is consistent with band-structure calculations. The abrupt change of the resistivity beyond 15 GPa suggests the mechanism of charge transport changes, which might be due to the pressure-induced phase transition. The resistivity beyond 23 GPa is within the order of magnitude of metallic values, suggesting a semiconductor-to-metal transition at much higher pressures that reported before [16,17]. The resistivity as a function of pressure can be divided into three regions. At low-pressure, the resistivity change from $\rho = 1.25 \times 10^9$ Ω cm to $\rho = 1.58 \times 10^4$ Ω cm is due to the decrease of the band gap. Then, in the region of phase coexistence it decreases from these values to $\rho = 12.5$ Ω cm, as the semiconductor and metallic phases coexists; and finally, resistivity has values around $\rho = 0.28$ Ω cm in the HP metallic phase. The pressure-induced metallization of HfSe$_2$ is verified by temperature-dependent resistance measurements discussed in the following section. Beyond 26 GPa, the change of resistance is negligible, and it remains almost pressure independent with a value 0.21 Ω cm.

To verify the pressure-induced metallization and achieve a more comprehensive understanding of electrical properties, temperature-dependent resistivity measurements were carried out down to 2 K from 5 GPa up to 38 GPa, as shown in Figs. 1(b), Fig. 2(d) and S1(Sup.
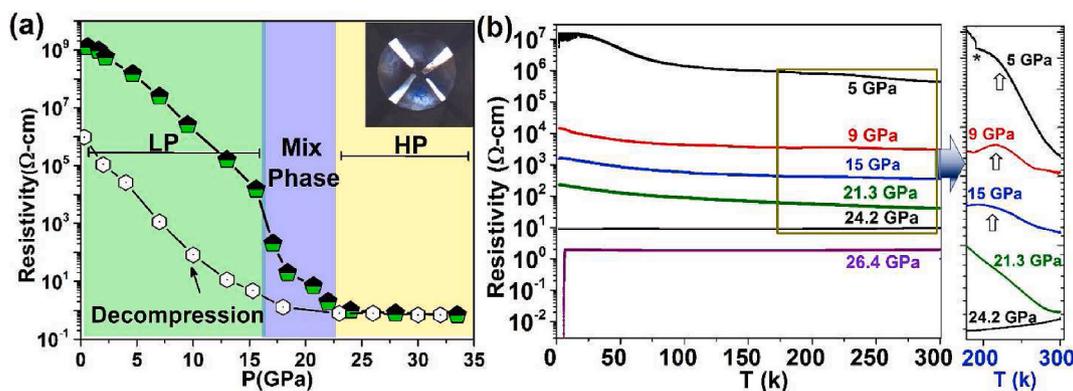
Fig. 1. (Color online); (a) Resistivity behavior of HfSe$_2$ as a function of pressure at RT. Regions corresponding to different phases are shown in green, blue, and yellow. A picture of the sample and contacts is shown in the inset. (b) Temperature-resistivity curves at different pressures, numbers show pressures in GPa. The asterisk in the zoom indicates the jump caused by changing the cooling speed while arrow indicating the CDW order.

Mat.); three regimes can be identified upon compression. Firstly, below 20 GPa, a typical semiconductor behavior is observed as it exhibits negative dρ/dT throughout all temperatures. Interestingly, it exhibited an anomalous behavior between 150 and 250 K, as indicated by the arrows in the inset of Fig. 1(b). The existence of a hump-type anomaly (a negative differential resistance) in the resistivity data is not unexpected for TMDs and it has been related to the presence of a weak CDW order in these materials [35]. Such phenomenon results in a crossover on the temperature-dependent transport behavior due to the electronic scattering by a CDW which affect the electronic density of states, changing the resistance-temperature slope [35–38]. The CDW behavior persists up

to at least 15 GPa and is almost suppressed with further compression at about 21.3 GPa. Secondly, at 24 GPa a positive dρ/dT is observed for all temperatures, implying the metallic behavior of HfSe$_2$. Thirdly, from 26 GPa to the highest pressure of 38 GPa, the resistivity shows a metallic state (dρ/dT > 0) between 300 K and 7 K. Interestingly, at 26 GPa we observed a sudden drop in resistance below 7 K, which suggests a pressure-induced superconductivity (SC) with a superconducting T_c of 6.6 K at 26 GPa. Further compression increases the T_c from 6.6 K to 7.5 K at 38 GPa, as presented in Fig. 2 (See Fig. S1(c) in Sup. Mat. For a zoom of the 29–38 GPa range). These results show that superconductivity is observed only at pressures beyond the pressure where the CDW state is
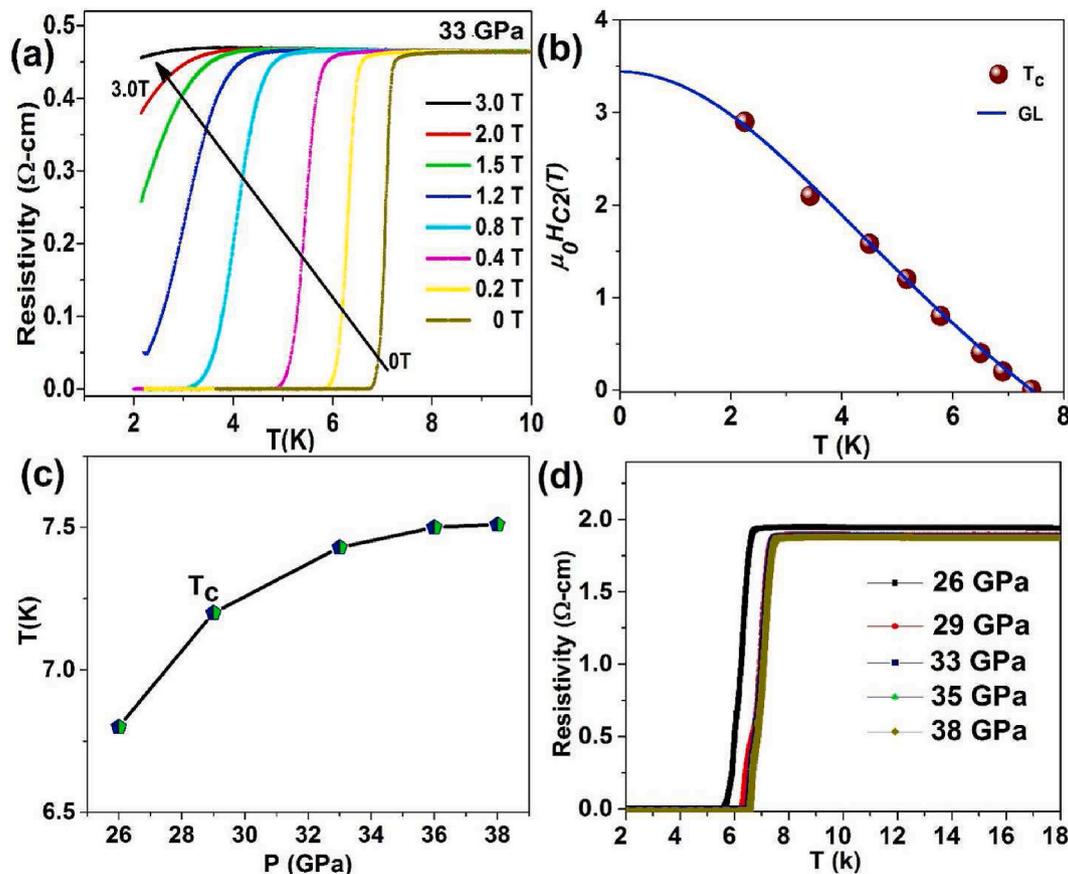
Fig. 2. (Color online) (a)Temperature dependence of resistivity under different magnetic fields (b) $\mu_0 H_{c2}$-T phase diagram. The solid line represents fitting by the GL equation. (c) Variation of T_c with increase pressure (d) Electrical resistivity as a function of temperature for pressures of 26–38 GPa. Electrical resistivity drops and zero-resistance at low T are an indication of superconductivity. A zoom of Fig. 2(d) is provided in Fig. S1(c) of Sup. Material.

suppressed [39]. The competition between both states is related to the fact that CDW order gaps out certain regions of the Fermi surface, and as such, the suppression of the CDW order leads to an enhancement of the superconducting transition temperature.

Superconductivity is further verified by the suppression of the T_c with increasing magnetic field (Fig. 2(a).). Zero resistance at 33 GPa is gradually lifted as the applied magnetic field increases, and simultaneously, the T_c decreases towards low temperature. The superconducting state is almost fully suppressed at the applied magnetic field of 3.4 T. In Fig. 2(b), we show the upper critical magnetic field, Hc2, determined from the onset of the resistivity drop [40]. The Hc2 vs. T_c curve was then fitted with the empirical expression based on the Ginzburg-Landau (GL) theory (e.g. Refs. [40,41]) which takes the form:

$$\mu_0 H_{c2}(T) = \mu_0 H_{c2}(0) \frac{1 - \left(\frac{T}{T_c}\right)^2}{1 + \left(\frac{T}{T_c}\right)^2} \qquad (1)$$

It can be seen that the data in Fig. 2(b) can be well-fitted using Eq. (1). The value of $\mu_0 H_{c2}(0)$ at 33 GPa is determined to be 3.4 T. We note that our derived value of $\mu_0 H_{c2}(0)$ is much lower than the Pauli limiting field for a singlet pairing of $\mu_0 H_P(0) = 1.84 T_c$ [42], which is 13.6 T for T_c = 7.4 K.

Another interesting feature is the variation of the superconducting critical temperature T_c with pressure, shown in Fig. 2(c) and (d). The superconducting transition temperature increases from 6.6 K to 7.5 K with increasing pressure then gradually levels off at 38 GPa.
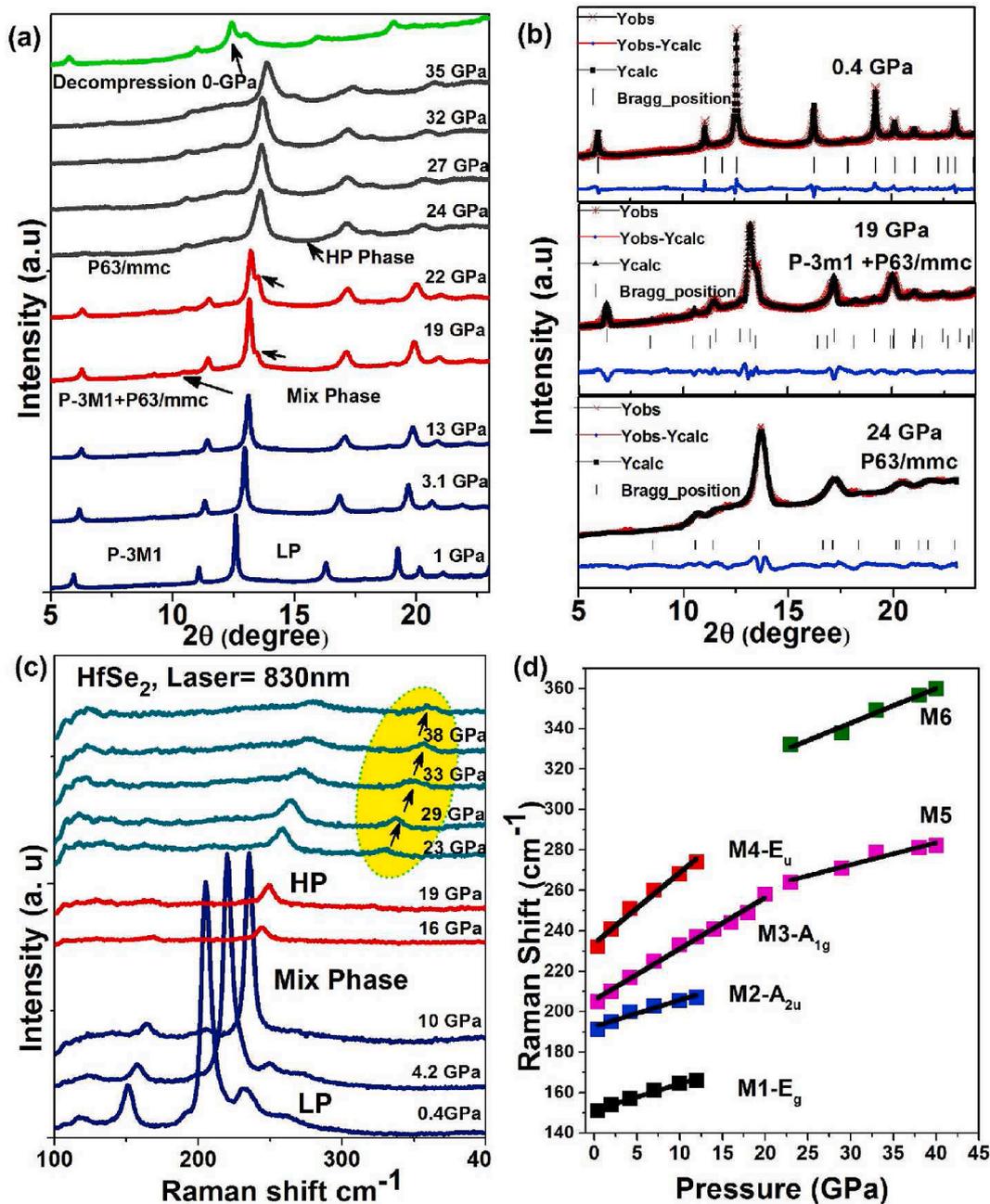
Fig. 3. (Color online) (a) Angle-dispersive XRD patterns at selected pressures at room temperature. (b) Rietveld refinements for the ambient phase, mixed phase, and new HP phase at 0.4 GPa, 19 and 24 GPa, respectively ($\lambda = 0.6199$ Å). (c) Raman spectra at different pressures between 0.4 and 38 GPa, (d) Pressure dependence of the Raman modes at different pressures between 1 atm and 38 GPa, where the solid lines show the linear fits corresponding to the specific modes.

3.2. Structural phase transition under compression

To reveal the structural origin of superconductivity and other interesting transport behavior of 1T-HfSe$_2$, we examined the crystal structure of the sample by high-pressure XRD measurements up to 35 GPa. XRD patterns are shown in Fig. 3(a). 1T-HfSe$_2$ crystallizes in a trigonal structure with space group P$\overline{3}$m1 at ambient pressure. XRD patterns up to 18 GPa can properly be refined with the same structure; see a representative refinement of the XRD patterns at 0.6 GPa in Fig. 3 (b). All XRD peaks are continuously shifted to a larger angle without the appearance of new peaks up to 18 GPa. After this pressure, additional diffraction peaks, indicated by arrows in the figure, started to appear. The new peaks become more prominent just over 22 GPa. This fact and the changes in the shape and intensity of the several peaks indicate the onset of a phase transition.

The superposition of the low- and high-pressure phases is observed in a pressure range of 19–23 GPa. At 24 GPa, prominent changes occur in the XRD pattern, which was refined by the hexagonal space group $P6_3/mmc$ and with further compression up to 35 GPa, no prominent change in the XRD pattern confirms the stability of the high-pressure phase. Representative Rietveld refinements of the HP-XRD patterns at 19 and 24 GPa are provided in Fig. 3(b). The low-pressure trigonal phase supports semiconducting behavior, and the pressure dependence of the conductivity supported the metallic behavior of the high-pressure hexagonal phase. The pressure-induced changes in the lattice parameter and unit-cell volume before and after the phase transition are discussed in Supplemental Material (Note 6). The discontinuity of the volume around 24 GPa (see Fig. S5 in Sup. Mat.) confirms the existence of a phase transition, which could trigger changes in the electronic topology. The transition is partially reversible and has the signature of a HP phase (see Fig. 3(a)). It is worth noting that the phase transition sequence found in this study is in good agreement with previous XRD measurements [17], although the authors could not solve the intermediate phase as it was mixed with 1T-phase and/or HP phase. In our study, a careful loading to avoid sample bridging [43] enable us to obtain the HP phase as a single phase from 24 to 32 GPa. We identified it with space group $P6_3/mmc$. This is consistent with our Raman experiments as we will show in the following paragraphs.

Raman spectra of HfSe$_2$ as a function of pressure at room temperature are shown in Fig. 3(c). They qualitatively agree with previous studies in the pressure range where comparable [32,44,45]. All the modes shift to higher frequency as the pressure increases. The peak intensity of main Raman modes especially A$_{1g}$ shows a jump with compression after 16 GPa as compared to the ambient Raman spectrum. This is due to phase coexistence, which has been observed in XRD measurements. Upon compression to 23 GPa, the appearance of the two new modes, a discontinuity in the pressure shift of one mode, as well as changes in the rate of mode-shift versus pressure in another mode indicate the lowering of crystalline symmetry, which corroborates the transition from trigonal (semiconductor) to hexagonal (metallic) as detected by XRD and electrical transport measurements. Indeed, the appearance of new modes cannot be explained by the tetragonal structure proposed in a previous work, which has the same number of Raman-active modes than the low-pressure phase. In contrast, calculations show that the $P6_3/mmc$ HP phase has four Raman-active modes (A$_{1g}$ + 2E$_{2g}$ + E$_{1g}$). The calculated Raman frequencies for the observed mode (242, 286 cm^{-1}) are almost equal to the experimental values (240, 290 cm^{-1}). Detailed information about these Raman modes is illustrated in the Supplemental Material (Note 4). The pressure evolution of the Raman modes is shown in Fig. 3(c–d) and illustrating the lowering of the crystalline symmetry. Upon decompression, the Raman spectrum is recovered to the original one at 0.2 GPa, as shown in Fig. S2 (Sup. Material), manifesting the partially reversible structural transition, in consistent with the observation of our XRD measurements.

3.3. Interpretation by density-functional theory calculations

To gain a better understanding of the electronic evolution of 1T-HfSe$_2$ in which its highly tunable optical and transport properties are determined, we carried out *ab-initio* calculations. Results from the structural optimization are shown in the Supplemental Material (Fig. S3, Sup. Material). According to these results, in the pressure range of interest of our study, the hexagonal HP structure ($P6_3/mmc$) has a higher enthalpy that the ambient-pressure trigonal structure (P$\overline{3}$m1). Thus, the $P6_3/mmc$ transition is found in calculations to be a metastable phase. In contrast, calculations predict a transition to a tetragonal structure (space group $I4/mmm$) at 16 GPa (see Fig. S3 in Sup. Material), in agreement with calculations previously reported. However, this tetragonal structure cannot explain the XRD patterns of the HP phase (see Fig. S4 in Sup. Material where we show the tetragonal structure has a very different XRD pattern). The fact that a different structural sequence is experimentally observed could be related to the existence of kinetic barriers blocking the P$\overline{3}$m1-$I4/mmm$ transition [46]. This transition is reconstructive and involves the formation of many Hf–Se bond (the coordination number in the tetragonal phase is 10) and the formation of Se–Se bonds (see Fig. S3 in Sup. Material). In contrast the $P6_3/mmc$ structure only differentiates from the low-pressure P$\overline{3}$m1 in the stacking of the stacked 2D HfSe$_2$ layers, which provide a simple mechanism to transform the P$\overline{3}$m1 structure into the $P6_3/mmc$ structure. Thus, the presence of kinetic barriers favors the stabilization of the $P6_3/mmc$ structure as a metastable phase. A detailed discussion of this issue is beyond the scope of this work. Despite this, the description of the DFT of the phonons and electronic properties of the low- and high-pressure phase with trigonal and hexagonal structures is accurate.

The electronic band structures and density of states (DOS) of the LP-phase were investigated by using an HSE06 hybrid functional at 1 atm, 5, 11, and 24 GPa, as shown in Fig. 4(a). The results clearly show a band gap narrowing in the low-pressure phase, which is consistent with the observations of transport measurements. At ambient pressure, our band structure calculations reveal a semiconducting ground state of HfSe$_2$ with an indirect band gap of about 0.82 eV, which is very close to the experimentally observed value of 0.8 eV (Fig. 4(a)). Under compression, the band-gap energy decreases to 0.2 eV at 5 GPa along with decreasing resistivity, as shown in Fig. 1(a). Above 5 GPa, there is a change in the slope of the resistivity, which is consistent with calculations showing HfSe$_2$ becomes a normal semimetal between 5 and 11 GPa, with the coexistence of electrons and hole pockets. From 11 to 24 GPa, the top of the valence band moves to 1 eV above the Fermi level, which justifies the decrease in resistivity by several orders of magnitude. Finally, the phase transition occurs at 24 GPa, and the sample becomes metallic with a resistivity of 10^{-1} Ω cm, as illustrated in Fig. 4(b). Thus, our calculations are fully consistent with our experiments. The semiconductor-semimetal transition can be interpreted as a symmetry-preserving phase transition, which modifies the topology of the band structure, similar to that reported for TiS$_2$ at 4–6 GPa [47]. From the projected DOS, we can see that the metallicity is derived mainly from the Hf *d* and Se *p* orbitals. Notice that the metallic character of the HP phase is fully consistent with the low intensity of its Raman signal.

We further calculated phonon spectra and EPC for $P6_3/mmc$ HfSe$_2$ at 29 GPa to provide an explanation of the observed superconductivity. The results are shown in Fig. S(7). The Eliashberg spectral function α^{2}F (ω)/ω between 2 and 7 THz have significant peaks, showing that the vibrations in this frequency range have a main contribution to the EPC. The calculated logarithmic average frequency ω$_{log}$ is 216 K and the EPC parameter λ is 0.34. To further explore the contribution of different phonon modes, red circles with the area proportional to the EPC strength are also plotted in the phonon dispersion curves. Most of the phonon modes along the Γ-A, H–K, and M-L direction have large contributions to the EPC, as well as the soft modes around the Γ point, which are associated with both Hf and Se atoms. The T_c of $P6_3/mmc$ HfSe$_2$ at 29 GPa
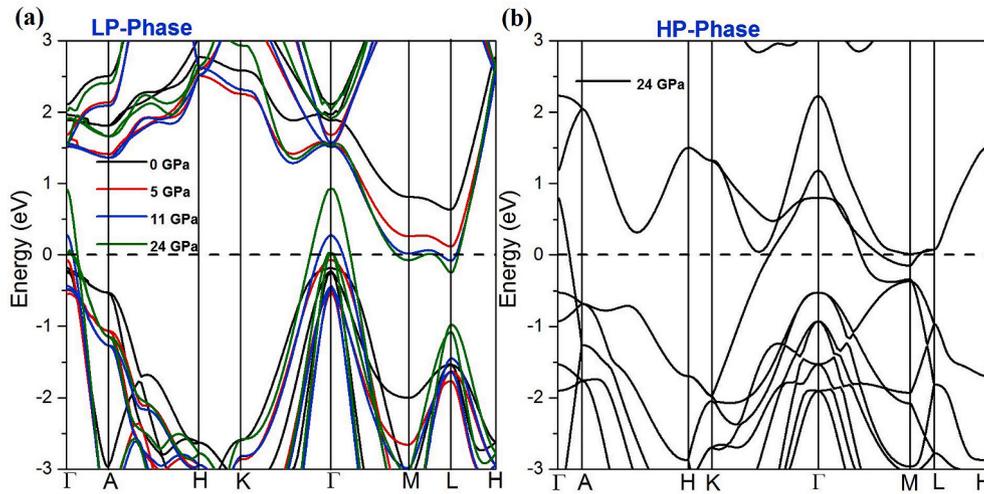
Fig. 4. (Color online) Calculated band structures of HfSe$_2$. (a) Ambient pressure (1atm), LP (5 GPa), LP (11 GPa), LP (24 GPa) (b) HP (24 GPa).

was calculated by using the Allen-Dynes modified McMillan equation. The estimated T_c is 0.7–2.8 K by applying a Coulomb pseudopotential μ^* of 0.1–0.13. The estimated low T_c is mainly due to the weak EPC and weak lattice vibrations. Although a discrepancy in T_c exists between the calculation and observation, it still qualitatively supports that $P6_3/mmc$ HfSe$_2$ is a superconductor at high-pressure.

Fig. 5 schematically illustrates the whole picture of this communication. Resistivity measurements, along with XRD and Raman spectroscopy, reveal a significant correlation between electronic, vibrational, and structural transitions in pristine 1T-HfSe$_2$ above 22 GPa. In the Raman spectrum and XRD patterns we noticed numerous changes, which provide strong evidence of a first-order structural transformation from trigonal (P $\bar{3}$ m1) to hexagonal $P6_3$/mmc around 24 GPa. In layered crystal structures like 1T-HfSe$_2$ there are strong van der Waals interactions between layers at ambient conditions. The

modification of van der Waals forces, which are highly sensitive to pressure, is usually accompanied by first-order structural transitions where massive structural reconstructions and atomic movements take place [48]. Therefore, in the case of HfSe$_2$, the metallization process involves the change in both the electronic and crystal structure. We believe that metallization phenomenon in HfSe$_2$ is intimately linked with the reduction of the pressure-induced interlayer distance. With compression, the distance of the neighboring Se atom planes decreased rapidly, resulting in the strong Se–Se interactions and further leads to the occurrence of metallization [49]. Our calculated electronic density of states (DOS); (see Fig S6); have shown that the density of the Se atoms around the Fermi level has significantly increased due to the enhancement of the interaction between the Se atoms under pressure. This is the key fact that drives metallization. Hf atoms also make a small contribution since the conduction band moves slightly down under pressure. Fig. 4 illustrates the complimentary evidence of the superconducting transition and metallization where the band structure of LP phase shows semiconducting behavior, and the HP phase shows metallic behavior. The fact that superconductivity is detected only after metallization is observed at room temperature implies that pressure-induced superconductivity is closely linked to the emergence of a first-ordered structural phase transition. Therefore, the superconductivity observed in HfSe$_2$ is an intrinsic phenomenon related to the structural changes observed in our experiments. The new approaches used in this article and the observed phase transitions involve versatile phase-control factors (such as temperature, pressure) creating new platforms and the resulting phases have also provided opportunities to explore novel 2D physics in the future.

4. Conclusions

1T-HfSe$_2$ undergoes a pressure-induced (P $\bar{3}$ m1 to $P6_3$/mmc) transformation near 24 GPa accompanied by a successive semiconductor-metal transition, resulting in the appearance of superconductivity at low temperature. This first-ordered phase transition is confirmed by Raman spectroscopy and the metallization associated with it by *ab-initio* electronic band structure calculations. The superconducting T_c increases gradually from ~6.5 K at 26 GPa to ~7.5 K at 38 GPa and becomes almost stable upon further compression. The extensive and continuous tuning of its electronic structure could be potentially used for energy-variable (IR-visible) optoelectronics and photovoltaics applications.

Fig. 5. Schematic pressure-temperature (P–T) phase diagram of IT-HfSe$_2$. The yellow and red regions demarcate the semiconducting and metallic states, respectively, illustrating the low-pressure and high-pressure structural phases. The CDW order and superconductor regions are indicated by CDW and SC, respectively. Symbols represent experimental data points of region boundaries (Insets) Schematic representations of the LP and HP crystal structures. White and Red circles represent Hf and Se, respectively. Stars indicates the resistivity behavior of HfSe$_2$ as a function of pressure at RT. The dashed-line box has been included to represent that structural determination has not been carried out at low temperature.

Declaration of competing interest

The authors declare that they have no known competing financial interests or personal relationships that could have appeared to influence the work reported in this paper.

Acknowledgements

Appendix A. Supplementary data

Supplementary data to this article can be found online at https://doi.org/10.1016/j.mtphys.2022.100698.

References

[1] M.N. Ali, J. Xiong, S. Flynn, J. Tao, Q.D. Gibson, L.M. Schoop, et al., Large, non-saturating magnetoresistance in WTe2, Nature 514 (2014) 205.

[2] I. Pletikosić, M.N. Ali, A.V. Fedorov, R.J. Cava, T. Valla, Electronic structure basis for the extraordinary magnetoresistance in WTe2, Phys. Rev. Lett. 113 (21) (2014) 216601.

[3] Y.I. Joe, X.M. Chen, P. Ghaemi, K.D. Finkelstein, G.A. de la Peña, Y. Gan, et al., Emergence of charge density wave domain walls above the superconducting dome in 1T-TiSe2, Nat. Phys. 10 (2014) 421.

[4] Z. Chi, X. Chen, F. Yen, F. Peng, Y. Zhou, J. Zhu, et al., Superconductivity in pristine 2Ha−MoS2 at ultrahigh pressure, Phys. Rev. Lett. 120 (3) (2018) 37002.

[5] Z. Ye, T. Cao, K. O'Brien, H. Zhu, X. Yin, Y. Wang, et al., Probing excitonic dark states in single-layer tungsten disulphide, Nature 513 (2014) 214.

[6] C.S. Snow, J.F. Karpus, S.L. Cooper, T.E. Kidd, T.C. Chiang, Quantum melting of the charge-density-wave state in 1T−TiSe2, Phys. Rev. Lett. 91 (13) (2003) 136402.

[7] H. Yuan, M.S. Bahramy, K. Morimoto, S. Wu, K. Nomura, B.-J. Yang, et al., Zeeman-type spin splitting controlled by an electric field, Nat. Phys. 9 (9) (2013) 563–569.

[8] Y. Zhang, T.-R. Chang, B. Zhou, Y.-T. Cui, H. Yan, Z. Liu, et al., Direct observation of the transition from indirect to direct bandgap in atomically thin epitaxial MoSe2, Nat. Nanotechnol. 9 (2) (2014) 111–115.

[9] C. Wang, B. Lian, X. Guo, J. Mao, Z. Zhang, D. Zhang, et al., Type-II ising superconductivity in two-dimensional materials with spin-orbit coupling, Phys. Rev. Lett. 123 (12) (2019) 126402.

[10] H. Yuan, X. Wang, B. Lian, H. Zhang, X. Fang, B. Shen, et al., Generation and electric control of spin–valley-coupled circular photogalvanic current in WSe2, Nat. Nanotechnol. 9 (10) (2014) 851–857.

[11] D.Y. Qiu, F.H. da Jornada, S.G. Louie, Optical spectrum of MoS2: many-body effects and diversity of exciton states, Phys. Rev. Lett. 111 (21) (2013) 216805.

[12] W.S. Yun, S.W. Han, S.C. Hong, I.G. Kim, J.D. Lee, Thickness and strain effects on electronic structures of transition metal dichalcogenides: 2H-MX2 semiconductors (M = Mo, W; X = S, Se, Te), Phys. Rev. B 85 (3) (2012) 33305.

[13] Z. Zhao, H. Zhang, H. Yuan, S. Wang, Y. Lin, Q. Zeng, et al., Pressure induced metallization with absence of structural transition in layered molybdenum diselenide, Nat. Commun. 6 (2015) 7312.

[14] Z.-H. Chi, X.-M. Zhao, H. Zhang, A.F. Goncharov, S.S. Lobanov, T. Kagayama, et al., Pressure-induced metallization of molybdenum disulfide, Phys. Rev. Lett. 113 (3) (2014) 36802.

[15] Y.Y. Hui, X. Liu, W. Jie, N.Y. Chan, J. Hao, Y.-T. Hsu, et al., Exceptional tunability of band energy in a compressively strained trilayer MoS2 sheet, ACS Nano 7 (8) (2013) 7126–7131.

[16] A. Andrada-Chacón, Á. Morales-García, M.A. Salvadó, P. Pertierra, R. Franco, G. Garbarino, et al., Pressure-driven metallization in hafnium diselenide, lnorg. Chem. 60 (3) (2021) 1746–1754.

[17] X. Zhang, B. Liu, S. Liu, J. Li, R. Liu, P. Wang, et al., Semiconductor-to-metal transition in HfSe2 under high pressure, J. Alloys Compd. 867 (2021) 158923.

[18] M.J. Mleczko, C. Zhang, H.R. Lee, H.-H. Kuo, B. Magyari-Köpe, R.G. Moore, et al., HfSe2 and ZrSe2: two-dimensional semiconductors with native high-κ oxides, Sci. Adv. 3 (8) (2017): e1700481.

[19] S.H. Chae, Y. Jin, T.S. Kim, D.S. Chung, H. Na, H. Nam, et al., Oxidation effect in octahedral hafnium disulfide thin film, ACS Nano 10 (1) (2016) 1309–1316.

[20] Q.H. Wang, K. Kalantar-Zadeh, A. Kis, J.N. Coleman, M.S. Strano, Electronics and optoelectronics of two-dimensional transition metal dichalcogenides, Nat. Nanotechnol. 7 (11) (2012) 699–712.

[21] Y. Jing, B. Liu, X. Zhu, F. Ouyang, J. Sun, Y. Zhou, Tunable electronic structure of two-dimensional transition metal chalcogenides for optoelectronic applications, Nanophotonics 9 (7) (2020) 1675–1694.

[22] A. Dewaele, M. Torrent, P. Loubeyre, M. Mezouar, Compression curves of transition metals in the Mbar range: experiments and projector augmented-wave calculations, Phys. Rev. B 78 (10) (2008) 104102.

[23] H. Mao, J.-A. Xu, P. Bell, Calibration of the ruby pressure gauge to 800 kbar under quasi-hydrostatic conditions, J. Geophys. Res. Solid Earth 91 (B5) (1986) 4673–4676.

[24] S. Klotz, J.C. Chervin, P. Munsch, G. Le Marchand, Hydrostatic limits of 11 pressure transmitting media, J. Phys. Appl. Phys. 42 (7) (2009) 75413.

[25] D. Errandonea, Y. Meng, M. Somayazulu, D. Häusermann, Pressure-induced α→ω transition in titanium metal: a systematic study of the effects of uniaxial stress, Physica B 355 (1) (2005) 116–125.

[26] Y. Wang, J. Lv, L. Zhu, Y. Ma, Crystal structure prediction via particle-swarm optimization, Phys. Rev. B 82 (9) (2010) 94116.

[27] Y. Wang, J. Lv, L. Zhu, Y. Ma, CALYPSO: a method for crystal structure prediction, Comput. Phys. Commun. 183 (10) (2012) 2063–2070.

[28] J.P. Perdew, J.A. Chevary, S.H. Vosko, K.A. Jackson, M.R. Pederson, D.J. Singh, et al., Atoms, molecules, solids, and surfaces: applications of the generalized gradient approximation for exchange and correlation, Phys. Rev. B 46 (11) (1992) 6671–6687.

[29] G. Kresse, J. Furthmüller, Efficient iterative schemes for ab initio total-energy calculations using a plane-wave basis set, Phys. Rev. B 54 (16) (1996) 11169–11186.

[30] P. Giannozzi, S. Baroni, N. Bonini, M. Calandra, R. Car, C. Cavazzoni, et al., Quantum ESPRESSO: a modular and open-source software project for quantum simulations of materials, J. Phys. Condens. Matter 21 (39) (2009) 395502.

[31] J. Heyd, G.E. Scuseria, M. Ernzerhof, Hybrid functionals based on a screened Coulomb potential, J. Chem. Phys. 118 (18) (2003) 8207–8215.

[32] R. Yue, A.T. Barton, H. Zhu, A. Azcatl, L.F. Pena, J. Wang, et al., HfSe2 thin films: 2D transition metal dichalcogenides grown by molecular beam epitaxy, ACS Nano 9 (1) (2015) 474–480.

[33] Q. Yao, L. Zhang, P. Bampoulis, H.J.W. Zandvliet, Nanoscale investigation of defects and oxidation of HfSe2, J. Phys. Chem. C 122 (44) (2018) 25498–25505.

[34] D. Errandonea, E. Bandiello, A. Segura, J.J. Hamlin, M.B. Maple, P. Rodriguez-Hernandez, et al., Tuning the band gap of PbCrO4 through high-pressure: evidence of wide-to-narrow semiconductor transitions, J. Alloys Compd. 587 (2014) 14–20.

[35] Z.-Y. Cao, J.-W. Hu, A.F. Goncharov, X.-J. Chen, Nontrivial metallic state of MoS2, Phys. Rev. B 97 (21) (2018) 214519.

[36] E. Piatti, Q. Chen, M. Tortello, J. Ye, R.S. Gonnelli, Possible charge-density-wave signatures in the anomalous resistivity of Li-intercalated multilayer MoS2, Appl. Surf. Sci. 461 (2018) 269–275.

[37] M. Mandal, S. Marik, K.P. Sajilesh, Arushi, D. Singh, J. Chakraborty, et al., Enhancement of the superconducting transition temperature by Re doping in Weyl semimetal MoTe2, Phys. Rev. Mater. 2 (9) (2018) 94201.

[38] A. Luican-Mayer, Y. Zhang, A. DiLullo, Y. Li, B. Fisher, S.E. Ulloa, et al., Negative differential resistance observed on the charge density wave of a transition metal dichalcogenide, Nanoscale 11 (46) (2019) 22351–22358.

[39] A.M. Gabovich, A.I. Voitenko, J.F. Annett, M. Ausloos, Charge- and spin-density-wave superconductors, Supercond. Sci. Technol. 14 (4) (2001) R1–R27.

[40] P. Müller, I.V. Grigorieva, V.V. Schmidt, A.V. Ustinov, The Physics of Superconductors: Introduction to Fundamentals and Applications, Springer Berlin Heidelberg, 2013.

[41] L. Fang, Y. Wang, P.Y. Zou, L. Tang, Z. Xu, H. Chen, et al., Fabrication and superconductivity of NaxTaS2 crystals, Phys. Rev. B 72 (1) (2005) 14534.

[42] A.M. Clogston, Upper limit for the critical field in hard superconductors, Phys. Rev. Lett. 9 (6) (1962) 266–267.

[43] D. Errandonea, A. Muñoz, J. Gonzalez-Platas, Comment on "High-pressure x-ray diffraction study of YBO3/Eu3+, GdBO3, and EuBO3: pressure-induced amorphization in GdBO3", J. Appl. Phys. 115 (2014) 43507. J Appl Phys 2014, 115 (21): 216101.

[44] L. Yin, K. Xu, Y. Wen, Z. Wang, Y. Huang, F. Wang, et al., Ultrafast and ultrasensitive phototransistors based on few-layered HfSe2, Appl. Phys. Lett. 109 (21) (2016) 213105.

[45] M. Kang, S. Rathi, I. Lee, L. Li, M.A. Khan, D. Lim, et al., Tunable electrical properties of multilayer HfSe2 field effect transistors by oxygen plasma treatment, Nanoscale 9 (4) (2017) 1645–1652.

[46] C. Cazorla, D. Errandonea, Ab initio study of compressed Ar(H2)2: structural stability and anomalous melting, Phys. Rev. B 81 (10) (2010) 104108.

[47] D.R. Allan, A.A. Kelsey, S.J. Clark, R.J. Angel, G.J. Ackland, High-pressure semiconductor-semimetal transition in TiS2, Phys. Rev. B 57 (9) (1998) 5106–5110.

[48] H. Yang, S.W. Kim, M. Chhowalla, Y.H. Lee, Structural and quantum-state phase transitions in van der Waals layered materials, Nat. Phys. 13 (10) (2017) 931–937.

[49] D. Errandonea, D. Martínez-García, A. Segura, A. Chevy, G. Tobias, E. Canadell, et al., High-pressure, high-temperature phase diagram of InSe: a comprehensive study of the electronic and structural properties of the monoclinic phase of InSe under high pressure, Phys. Rev. B 73 (23) (2006) 235202.